

## Modelling azimuthal NMO in laterally heterogeneous HTI media

Edward Jenner,<sup>\*</sup> ION Geophysical, expands previous work on how lateral velocity heterogeneity in the overburden could explain apparent azimuthal NMO at a target horizon on field data. Here, modelling studies show, among other things, that lateral variations in anisotropy are well resolved and do not distort the inverted interval anisotropy in deeper target layers if the vertical velocity is laterally homogeneous.

For traveltimes data, it is known that lateral heterogeneity can manifest itself as anisotropy (Grechka, 1998; Grechka and Pech, 2006), potentially distorting inversion and interpretation of derived medium properties. Jenner (2008) modelled lateral velocity variations less than the scale of a CMP spread and concluded that the distortions in effective NMO ellipses are not suppressed by Dix-type conversion to interval NMO ellipses. In addition, this modelling also demonstrated that a particular azimuthal velocity anomaly observed in field data could potentially be explained solely by lateral velocity variations in an isotropic overburden. A characteristic of isotropic models containing lateral heterogeneities was that effective (RMS) and interval NMO ellipses were highly correlated and displayed similar patterns as the lateral heterogeneities, even when those heterogeneities were quite complex.

In azimuthal velocity analysis, regions of anomalous azimuthal NMO magnitude and/or direction are often of most interest to the interpreter, and many authors have indeed shown strong variations in azimuthal anisotropy (e.g., Cardona et al., 2003; Xiang-Yang et al., 2003; Al-Marzoug et al., 2006; Sun et al., 2006; Wang et al., 2007). Even in areas of relatively mild lateral velocity variations, laterally heterogeneous anisotropy cannot always be expected to be

confined to the target interval. Mechanisms that produce lateral variations in anisotropy, such as changes in horizontal stress due to basement faulting, can be expected to operate over a wide range of depths. So it can be seen that the nature of the anisotropy may vary as the lithology and structural setting changes.

This paper investigates the azimuthal NMO response for models that contain combinations of both laterally heterogeneous anisotropy and laterally heterogeneous vertical velocity. In general the effective azimuthal NMO signatures are more complicated than the simple case of a single isotropic but laterally heterogeneous layer. However, in the case of two layers exhibiting horizontal transverse isotropy (HTI) and containing lateral variations in anisotropy but not in vertical velocity, the laterally varying anisotropy is recovered in both intervals. This situation might occur, for instance, in the case of vertical, aligned cracks varying in crack density in a homogeneous background medium. On the other hand, when the overburden contains either isotropic lateral velocity variations, or lateral variations in vertical velocity in an HTI medium, the heterogeneity causes distortions in the interval NMO ellipses at subsequent HTI layers. In this case the overburden heterogeneity must be accounted for in the analysis of azimuthal anisotropy.

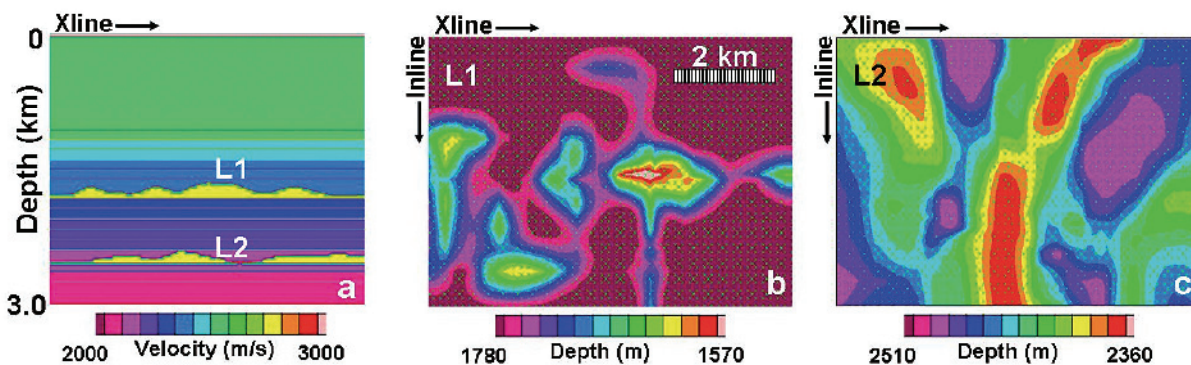
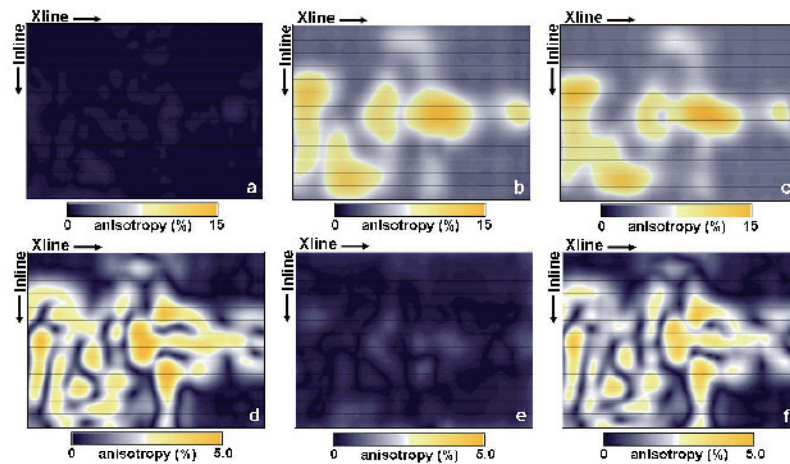


Figure 1 a) Inline profile through centre of model. The velocity structure consists of two layers with topographic variation embedded in a  $V(z)$  background medium. The two topographic layers are shown in yellow. b) and c) Depths to top of the first (L1) and second (L2) topographic layers respectively.

<sup>\*</sup> [edward.jenner@iongeo.com](mailto:edward.jenner@iongeo.com)



**Figure 2** Time slices through the interval anisotropy at L1 (a, b, and c) and 600 ms below L1 (d, e, and f) for models where lateral heterogeneities are confined to TL1 only. a) and d) Model with lateral variation in velocity, but not anisotropy. b) and e) Model with lateral variation in anisotropy, but not in the vertical velocity; and c) and f) model with lateral variations in both anisotropy and vertical velocity.

**Method**

Geologic models were created by embedding two reflectors with topography in a laterally homogeneous medium with velocity increasing with depth as depicted in Figure 1. For the various models, HTI anisotropy (N-S isotropy plane) and/or vertical velocity contrast is introduced between one or both of the topographic layers (coloured yellow in Figure 1a) and the surrounding medium. This effectively creates two layers with lateral variations in isotropic (or vertical) velocity and/or lateral variations in azimuthal anisotropy.

Initially models were created with only the first layer, named L1, present. The first of these models was isotropic with lateral variations in velocity in this layer. This model was then compared with two anisotropic models, T2 and T3. The first layer parameters for the anisotropic models T2 and T3 are given in Table 1, along with the parameters for model T1. The  $\epsilon$  and  $\delta$  parameters are defined using the notation of Thomsen (1986) for a rotated vertical transverse isotropic (VTI) medium with the  $x_3$  axis pointing in the (horizontal) symmetry direction (Rüger 1997). Using Rüger (1997), they can be related to the HTI parameters  $\epsilon^{(v)}$  and  $\delta^{(v)}$ . Note that the azimuthal

anisotropy measured as the variation in NMO velocity in the horizontal plane is determined by  $\delta^{(v)}$  for an HTI medium. In Table 1,  $V_0$ (HTI) is the vertical velocity in the HTI medium and  $V_h$ (HTI) is the velocity perpendicular to the isotropy plane (i.e., perpendicular to the ‘fractures’). For this layer the background medium velocity is 2200 m/s. Thus T1 is isotropic with lateral velocity heterogeneity; T2 is anisotropic with lateral variation in anisotropy, but not in the vertical velocity; and T3 is laterally heterogeneous in both anisotropy and vertical velocity.

Subsequently, models with both the first and second heterogeneous layers were created. For the initial models, T2 and T3 azimuthal anisotropy was added to the second layer with  $\epsilon = \delta = 0.1$ . In addition, a model containing only the second layer was generated as a baseline comparison.

These models were then ray-traced, generating specular reflections with a simple, regular square pattern of sources and receivers. The source wavelet had a frequency band from 10 to 50 Hz. For the purposes of this experiment, and in the interests of time, diffractions were not modelled, and subsequently the data were not migrated prior to azimuthal velocity analysis. In addition, discontinuities in the models, non-zero ray capture radii and other numerical artefacts resulted in some small errors being introduced into the traveltimes and thus the inversion. Note that ray-tracing does not account for wavefront healing, scattering, multiples and finite-frequency effects.

The method used for picking and inverting traveltimes is described in detail in Jenner (2001) and summarized by Jenner et al. (2001). It is a windowed cross-correlation technique that aims to provide relative trace-to-trace time shifts within a normal moveout (NMO) corrected gather as a function of zero-offset traveltime. These time shifts are then used to compute total traveltimes as a function of offset and azimuth at the chosen zero-offset times which are then inverted for the azimuthal variation in NMO velocity.

Grechka and Tsvankin (1998) showed that within the range of offsets where the traveltimes are approximately hyperbolic

	T1	T2	T3
$\epsilon$	0	0.15	0.15
$\delta$	0	0.15	0.15
$V_0$ (HTI)	1930	2200	1930
$V_h$ (HTI)	1930	1930	1692

**Table 1** Thomsen (1986) parameters and velocities for the three models containing lateral heterogeneity in the first layer.  $V_0$ (HTI) and  $V_h$ (HTI) are the vertical and horizontal velocities respectively in the rotated VTI medium (i.e. in the HTI medium).

and increasing with offset, the azimuthal variation of pure-mode NMO velocity will be elliptical, independent of the subsurface geology. The reflection moveout of pure (non-converted) modes can be approximated by the hyperbolic equation:

$$T^2 = T_0^2 + \frac{X^2}{V_{nmo}^2(\phi)},$$

where

$$\frac{1}{V_{nmo}^2(\phi)} = \frac{1}{V_{slow}^2} \cos^2(\phi - \beta_s) + \frac{1}{V_{fast}^2} \sin^2(\phi - \beta_s).$$

$T$  is the total traveltime,  $T_0$  is the two way zero-offset traveltime,  $X$  is the offset,  $V_{fast}$  is the fast velocity (semi-major axis of the NMO ellipse),  $V_{slow}$  is the slow velocity (semi-minor axis of the NMO ellipse),  $\beta_s$  is the slow velocity azimuth and  $V_{nmo}(\phi)$  is the azimuthally varying velocity as a function of the source-receiver azimuth  $\phi$ .

Following Grechka and Tsvankin (1998) and Grechka et al. (1999), the total traveltime can then be written as

$$T^2 = T_0^2 + (W_{11} \cos^2 \phi + 2W_{12} \cos \phi \sin \phi + W_{22} \sin^2 \phi) X^2, \quad (1)$$

where  $W_j$  are the NMO ellipse coefficients and are functions of the azimuth of the slow velocity,  $\beta_s$ , and the fast and slow velocities ( $V_{fast}$  and  $V_{slow}$ ).

Using equation (1), a linear least squares inversion is first performed to solve for the ellipse coefficients,  $W_j$ . These coefficients are then directly related to the effective fast and slow velocities and the fast velocity azimuth. Interval ellipse coefficients are then obtained from effective coefficients using the Dix-type method described by Grechka et al. (1999) and these interval  $W_j$ s are similarly converted to the interval fast and slow velocities and interval fast velocity azimuth. Although the Dix-type method for computing interval parameters assumes lateral homogeneity, this method has been applied to all the modelling examples. More robust methods for determining interval anisotropy (or interval ellipses) exist, however, the Dix-type conversion is still more commonly used in practice. In addition, while the assumption of lateral homogeneity is violated in the models discussed in this paper, the stability and consistency of the interval parameters suggests that it is still a reasonable approximation for these models.

For the traveltime inversion, the data were limited to offset-to-depth ratios (ODRs) of 1.0. Although somewhat arbitrary, in practice for land seismic data, the moveout curves are generally hyperbolic within this offset range. Indeed, for hard-rock areas, where the velocity gradient is mild, one can often use ODRs up to 1.3 before the traveltimes begin to display non-hyperbolic moveout, which can improve the signal-to-noise ratio in the inversion of field data. The NMO ellipses for all synthetic models were obtained using the same procedure with the same time-shift picking and inversion parameters.

In Figures 2–5 the inverted NMO ellipses are characterized by their ‘anisotropy’, defined by:

$$\frac{V_{fast} - V_{slow}}{V_{fast}}$$

Note that for the HTI model  $V_{fast}$  is the same as the isotropic background velocity.

### Results

Time slices of the inverted interval anisotropies for the three initial models are compared in Figure 2 at L1, the first heterogeneous layer at 1700 ms and 600 ms below L1 at 2300 ms. Figure 2a shows that for the isotropic, heterogeneous model (T1) interval NMO ellipses at 1700 ms display almost zero azimuthal velocity variation. However, at later times, the influence of the lateral velocity variation becomes apparent as seen in Figure 2d. As discussed by Jenner (2008), the RMS and interval NMO ellipses are highly correlated, only slowly varying in time and display features related to the overburden heterogeneity. Although the anisotropy displays a rather complex pattern, the fast and slow velocity attributes individually correlate with specific portions of the overburden heterogeneity. Similarly the azimuth of the fast velocity also displays patterns that correlate with the overburden heterogeneity.

For model T2 Figures 2b and 2e show that the laterally varying interval anisotropy is resolved at 1700 ms within the resolution of the velocity analysis technique but is extremely weak at 2300 ms. Thus, the lateral variation in anisotropy does not result in an appreciable artificial apparent anisotropy below the anisotropic layer. In model T3, the two types of heterogeneity are combined, and the lateral variation in ani-

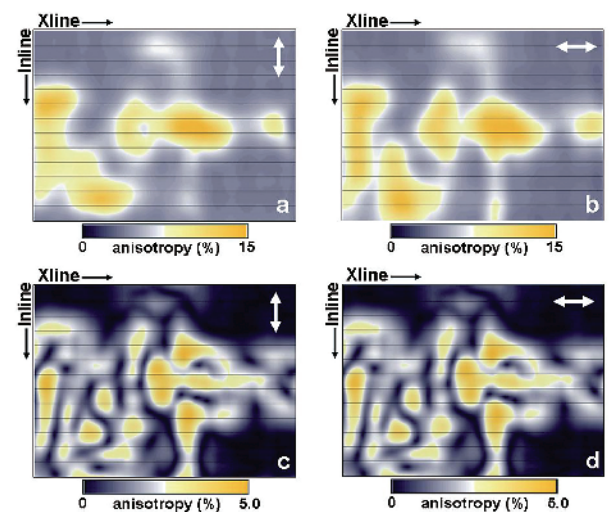
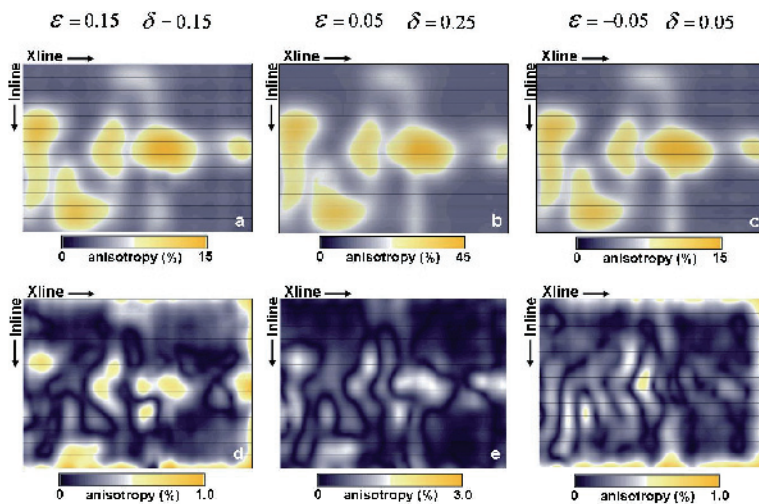


Figure 3 Time slices through the interval anisotropy at L1 (a and b) and 600 ms below L1 (c and d) for HTI models with the isotropy plane (fracture orientation) N-S (a and c) and E-W (b and d). Both models also include lateral variations in vertical velocity.

## Data Processing



**Figure 4** Time slices through the interval anisotropy at L1 (a, b, and c) and 600 ms below L1 (d, e, and f) for various HTI models. a) and d) Model with  $\epsilon = \delta = 0.15$ , b) and e) model with  $\epsilon = 0.25$ ,  $\delta = 0.05$  and c) and f) model with  $\epsilon = 0.05$ ,  $\delta = -0.05$ . Note the scale change between the upper and lower figures.

sotropy is again resolved at 1700 ms, but the lateral variation in vertical velocity also results in apparent interval azimuthal velocity anisotropy at 2300ms (Figures 2c and 2f respectively). As with model T1, at 2300 ms the parameters defining the NMO ellipses are correlated with the structure and therefore the lateral velocity variation. Note that the effective ellipses at 2300 ms in model T3 contain both the influence of the overlying anisotropy and the influence of lateral velocity variations. However, while the effective anisotropy at 2300 ms is different for models T1 and T3, apparent interval anisotropy at 2300 ms is extremely similar.

Variations in model parameters, for instance, rotating the anisotropy plane from North-South to East-West or changing the values of  $\epsilon$  and  $\delta$  yields similar results. When the anisotropy plane is rotated by  $90^\circ$  in model T3 (laterally heterogeneous anisotropy and vertical velocity), the effective NMO ellipses are also rotated by  $90^\circ$ . The inverted interval anisotropy for the model with the isotropy plane rotated is compared to the original model in Figure 3. At 1700 ms, both effective and interval ellipses are still similar, and the result of converting effective NMO ellipses to interval NMO ellipses, shown in Figures 3a and 3b, recovers the anisotropy. Note that there are some subtle differences due to the obtainable resolution using a CMP spread with an offset of  $\sim 2$  km. This is particularly evident with the N-S trending features which are better resolved when the isotropy plane is oriented perpendicular to the lateral heterogeneity.

As with model T3, at 2300 ms the effective ellipses are a combination of the effects of the rotated HTI medium and the lateral velocity variation. However, the interval ellipses at this time for the E-W isotropy plane model are almost identical to the original (N-S isotropy plane) model as seen by comparing Figures 3c and 3d. This supports the assertion that the apparent anisotropy below the heterogeneous layer

is induced primarily by the lateral variation in the vertical velocity, and not the variation in anisotropy.

So far, all the anisotropic models have exhibited elliptical anisotropy ( $\epsilon = \delta$ ). The elliptical case ( $\epsilon = \delta = 0.15$ ) is compared to two highly non-elliptical anisotropies, one with an extremely high azimuthal anisotropy in the horizontal plane ( $\epsilon = 0.25$ ,  $\delta = 0.05$ ) and one with a similar azimuthal anisotropy as the elliptical case ( $\epsilon = 0.05$ ,  $\delta = -0.05$ ). Figure 4 compares the results of inverting the interval azimuthal NMO velocity for these models at 1700 ms and 2300 ms. Note that in these models there is no lateral variation in the vertical velocity. Clearly in all models the interval anisotropy is well recovered at the anisotropic layer, even in the extreme case of  $\epsilon = 0.25$ ,  $\delta = 0.05$ . At 2300 ms there is a very small apparent anisotropy compared to the anisotropy at 1700 ms. Although the apparent anisotropies at 2300 ms display subtly different characteristics between the models, this residual is so small that it is unclear if this has any real significance. Thus, as expected from the previous results, when the vertical velocity is homogeneous, the interval anisotropy below the anisotropically heterogeneous layer is negligible.

An example of overburden distortion on the computed anisotropy of a layer is demonstrated in Figure 5. In this example, both L1 and L2 are anisotropic and thus there exists heterogeneity at both depths. L1 has the same HTI parameters as described previously for the initial models ( $\epsilon = \delta = 0.15$ ), and HTI anisotropy is introduced into L2 with anisotropy parameters  $\epsilon = \delta = 0.1$ . The vertical velocity in L2 is homogeneous and thus equal to the background velocity.

Figure 5a shows the result of inverting for the interval anisotropy at L2 if the vertical velocity in L1 is homogeneous, in other words, model T2 with L2 added. In this case the interval anisotropy is well resolved and is almost identical to the result obtained, but not shown, when L1 is removed

completely. However, when a laterally varying vertical velocity in L1 is introduced into the model, the anisotropy in L2 is distorted. Figure 5b shows the inverted interval velocity at L2 when the overburden layer, L1, contains the same model parameters as for model T3. This distortion is due to the addition of the apparent interval anisotropy at this depth introduced by the lateral variation in L1 as shown in Figure 2f. Thus, any distortion in L2 does not appreciably depend on the overburden anisotropy heterogeneity, but is heavily dependent on the magnitude of the lateral variation in vertical (or isotropic) velocity in the overburden.

Note that the distorted interval anisotropy at L2 is not simply an addition of the anisotropy shown in Figure 2f with the anisotropy at L2 shown in Figure 5a. This is demonstrated in Figure 5c which displays the differences between the distorted and undistorted anisotropy at L2. The reason for this is that the azimuths of the interval NMO ellipses for the apparent anisotropy induced by lateral variations in overburden vertical velocity are not omni-directional. Thus, the distortion of anisotropies is not a simple scalar addition of the apparent anisotropies, but a super-position of interval NMO ellipses. However, it is still clear that the distortion is related to the overburden lateral velocity variation since its shape displays similar characteristics to the induced apparent interval anisotropy (Figure 2f).

## Discussion

In this study, the influence of lateral velocity and anisotropy heterogeneities was modelled in a relatively simple fashion. The anisotropy was evaluated on horizontal reflections and the modelling was performed with simple specular ray-tracing with a regular grid of sources and receivers. This was deemed appropriate because of the simplicity of the models and a desire to avoid complicating or confusing the analysis.

In field data, however, even for horizontal layering, amplitude variations along reflectors may result in diffracted energy which could become an issue in picking traveltimes, resulting in additional distortions in the apparent anisotropy. In addition, there may be dipping reflections, and in both these cases prestack migration may be warranted to collapse diffractions and move events to their correct locations. This may also result in more complex phenomena not encountered in this study. Perhaps a bigger limitation of this study is the use of ray-tracing itself. Finite difference modelling

would likely produce different results, particularly in apparent anisotropy magnitudes, and possibly lateral resolution. In addition, finite difference modelling may also show more dependence on the precise nature of the lateral heterogeneities, for instance, whether the layer is a topographic feature as used here or simply a layer with lateral heterogeneities which could also be discontinuous.

Despite these shortcomings, it is clear from this study that overburden lateral heterogeneities in isotropic or vertical velocity must be accounted for if reliable anisotropic attributes are to be measured at a target horizon. Grechka and Tsvankin (1999) showed that in areas of mild dip, NMO ellipses at a target horizon may be corrected if the overburden heterogeneity is mild and is smoothly varying over a CMP spread length. For the types of lateral heterogeneities presented here, however, a method that can handle stronger lateral variations would be required.

The modelling study presented in this paper suggests that the effects of lateral variations in vertical velocity and anisotropy result in a super-position of effective and interval NMO ellipses. Thus it appears that the two effects are non-interacting and thus potentially separable. Prestack depth migration (PSDM) would be a natural choice if an accurate isotropic velocity model can be built. The ultimate solution would be a wide-azimuth anisotropic tomography that would simultaneously invert for the lateral velocity heterogeneity and the anisotropy in an intelligent manner. However, this might be subject to numerical instabilities and would need to ensure that lateral vertical velocity variations are not interpreted as anisotropy. An alternative and more straightforward workflow would be to build an isotropic or VTI depth model, iterating until no further improvements in flattening the events within common image point gathers are possible. This model should be built using wide-azimuth tomography since the azimuthal variations in velocity due to the overburden heterogeneity must be correctly accounted for. Once this has been achieved, one would then analyze the gathers for azimuthal anisotropy and possibly perform an azimuthally anisotropic PSDM.

Recently Dickinson and Ridsdill-Smith (2010) successfully applied a similar workflow to a multi-azimuth marine dataset. Their results supported the idea that the isotropic portion of the velocity field and anisotropy are indeed separable, even when both are laterally heterogeneous. Their

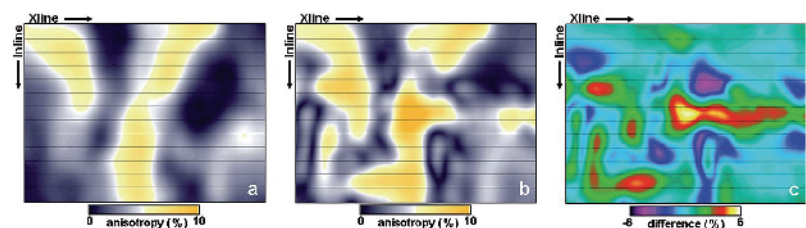


**Figure 5** a) and b) Time slices of interval anisotropy at TL2 for models with two heterogeneous layers. a) Result when both layers contain lateral variation in anisotropy, but no variation in vertical velocity. b) Result when TL1 also contains lateral variation in vertical velocity. c) The difference between the results in a) and b).

## Data Processing

model was relatively horizontally stratified with anomalous velocity lenses in the overburden. Thus it remains to be seen if this workflow could adequately handle areas of complex structure.

### Conclusions

Here it is shown that for an HTI medium with multiple anisotropic layers, laterally heterogeneous anisotropy may be well recovered by inverting traveltimes with a Dix-type conversion to interval NMO ellipses. However, this only holds as long as the vertical velocity does not display significant lateral variation as might be expected in the case of vertical fractures embedded in a homogeneous isotropic rock. In this case of homogeneous vertical velocity, the inverted interval azimuthal anisotropy is only significant at the anisotropic layers and is small elsewhere.

When lateral variations in the vertical velocity are introduced into a laterally heterogeneous anisotropic overburden, the apparent anisotropy below the heterogeneities is the same as for an isotropic overburden with the same heterogeneity in the isotropic velocity as the vertical velocity heterogeneity in the HTI medium. Thus it appears that the isotropic and anisotropic portions of the overburden may be separable. A proposed method for obtaining the correct anisotropy would be to perform isotropic PSDM until the model can no longer be refined, and then analyze the data for azimuthal anisotropy.

### Acknowledgements

I would like to thank ION for permission to publish this work and in particular David Jones for his help in putting together the manuscript.

### References

- Al-Marzoug, A. M., Neves, F. A., Kim, J. J. and Nebrija, E. L. [2006] P-wave anisotropy from azimuthal AVO and velocity estimates using 3D seismic data from Saudi Arabia. *Geophysics*, **71**, E7.
- Cardona, R., Jenner, E. and Davis, T. L. [2003] Fracture network characterization from P- and S-wave data at Weyburn field, Canada: Egypt. *76<sup>th</sup> SEG Annual Meeting*, Expanded Abstracts, **22**, 370.
- Dickenson, D. and Ridsdill-Smith, T. [2010], The Benefits of Multi-azimuth Depth Migration over the Tidepole Field, North West Shelf, Australia. *72<sup>nd</sup> EAGE Conference and Exhibition*, Barcelona.
- Grechka, V. and Pech A. [2006] Quartic reflection moveout in a weakly anisotropic dipping layer. *Geophysics*, **71**, D1-D13.
- Grechka, V. and Tsvankin, I. [1998] 3-D description of normal-moveout in anisotropic inhomogeneous media. *Geophysics*, **63**, 1079-1072.
- Grechka, V. and Tsvankin I. [1999] 3-D moveout inversion in azimuthally anisotropic media with lateral velocity variation: Theory and a case study. *Geophysics*, **64**, 1202-1218.
- Grechka, V., Tsvankin, I. and Cohen, J. K. [1999] Generalized Dix equation and analytic treatment of normal-moveout velocity for anisotropic media. *Geophysical Prospecting*, **47**, 117-148.
- Jenner, E. [2008] Data example and modelling study of P-wave azimuthal anisotropy potentially caused by isotropic velocity heterogeneity. *First Break*, **27**, 45-50.
- Jenner, E. [2001] Azimuthal anisotropy of 3D compressional wave seismic data. Ph.D. Thesis, Colorado School of Mines.
- Jenner, E., Williams, M. and Davis, T. [2001] A new method for azimuthal velocity analysis and application to a 3D survey, Weyburn field, Saskatchewan, Canada. *71<sup>st</sup> SEG Annual Meeting*, Expanded Abstracts, **20**, 102.
- Rüger, A. [1997] P-wave reflection coefficients for transversely isotropic media with vertical and horizontal axis of symmetry. *Geophysics*, **62**, 713-722.
- Sun, S., Johns M. K. and Zhou D. [2006] P-wave azimuthal velocity inversion for fracture detection in an East Texas gas field. *76<sup>th</sup> SEG Annual Meeting*, Expanded Abstracts, **25**, 130.
- Thomsen, L. [1986] Weak elastic anisotropy. *Geophysics*, **51**, 1954-1966.
- Wang, J., Zheng Y. and M. Perz, [2007] VVAZ vs. AVAZ: Practical implementation and comparison of two fracture-detection methods. *77<sup>th</sup> SEG Annual Meeting*, Expanded Abstracts, **26**, 189.
- Xiang-Yang, L., Liu, Y.-J., Liu, E., Shen, F., Qi, L. and Shouli, Q. [2006] Fracture detection using land 3D seismic data from the Yellow River Delta, China. *The Leading Edge*, 680-683.